

RSC Advances



This is an *Accepted Manuscript*, which has been through the Royal Society of Chemistry peer review process and has been accepted for publication.

Accepted Manuscripts are published online shortly after acceptance, before technical editing, formatting and proof reading. Using this free service, authors can make their results available to the community, in citable form, before we publish the edited article. This *Accepted Manuscript* will be replaced by the edited, formatted and paginated article as soon as this is available.

You can find more information about *Accepted Manuscripts* in the [Information for Authors](#).

Please note that technical editing may introduce minor changes to the text and/or graphics, which may alter content. The journal's standard [Terms & Conditions](#) and the [Ethical guidelines](#) still apply. In no event shall the Royal Society of Chemistry be held responsible for any errors or omissions in this *Accepted Manuscript* or any consequences arising from the use of any information it contains.

$\text{Li}_{2+x}\text{MnSi}_{1-x}\text{Al}_x\text{O}_4/\text{C}$ nanoparticles for high capacity lithium-ion battery cathode applications

Meng Zhang,^{*a} Shiju Zhao,^b Qiuling Chen^a and Guojin Yan^a

Abstract $\text{Li}_{2+x}\text{MnSi}_{1-x}\text{Al}_x\text{O}_4/\text{C}$ ($0 < x < 0.09$) nanoparticles were synthesized under supercritical fluid conditions at 550 °C for 3 h using water and ethanol as mixed solvent. Compared with $\text{Li}_2\text{MnSiO}_4$, $\text{Li}_{2+x}\text{MnSi}_{1-x}\text{Al}_x\text{O}_4$ displays higher theoretical capacity and better electrochemical properties. $\text{Li}_{2.09}\text{MnSi}_{0.91}\text{Al}_{0.09}\text{O}_4/\text{C}$ nanoparticles with an average diameter of ca. 11 nm deliver a high discharge capacity of 308 $\text{mAh}\cdot\text{g}^{-1}$, which indicates approximate two Li^+ ion exchange can be realized during the cycling process.

Introduction

Recently, lithium-ion batteries have attracted great interest due to their widely applications in mobile phones, laptop computers and other portable electronic devices. Especially, the lithium-ion batteries have been also considered to one of promising power sources for electric vehicles and hybrid-electric vehicles.¹⁻³ It is well known that the increased capacity of lithium-ion batteries can improve the performances of the above electronic and electric equipments. However, the low theoretical specific capacity of conventional cathode materials, such as LiCoO_2 ($274 \text{mAh}\cdot\text{g}^{-1}$), LiMn_2O_4 ($148 \text{mAh}\cdot\text{g}^{-1}$) and LiFePO_4 ($170 \text{mAh}\cdot\text{g}^{-1}$), limits the increase of battery capacity. Compared with conventional cathode materials, lithium metal silicate (Li_2MSiO_4 , $\text{M} = \text{Fe}, \text{Mn}, \text{Co}$ and Ni) have high theoretical specific capacity ($> 330 \text{mAh}\cdot\text{g}^{-1}$, which is possible while extracting two Li^+ ion per formula unit).

$\text{Mn}^{3+}/\text{Mn}^{4+}$ redox couples, due to its lower cell voltage,⁴ is convenient to study rather than $\text{Fe}^{3+}/\text{Fe}^{4+}$, $\text{Co}^{3+}/\text{Co}^{4+}$ or $\text{Ni}^{3+}/\text{Ni}^{4+}$. Therefore, $\text{Li}_2\text{MnSiO}_4$ can be a more suitable choice as one of high capacity cathodes. Up to now, some methods have been developed to optimize the electrochemical properties of $\text{Li}_2\text{MnSiO}_4$, for example, controlling the particle size and morphology,⁵⁻⁷ doping certain cations^{8,9} and surface

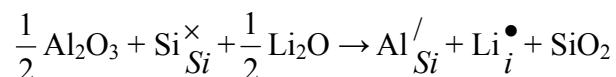
^a School of Materials Science and Engineering, Henan University of Technology, Zhengzhou 450007, China. E-mail: meng_zhang@haut.edu.cn

^b School of Science, Henan Agricultural University, Zhengzhou 450002, China.

coating with conductive materials,¹⁰⁻¹⁵ and the deintercalation of more than one Li⁺ ion already is achieved in Li₂MnSiO₄ cathodes, which makes Li₂MnSiO₄ show high capacity than other cathodes.¹⁶ Then, can the higher theoretical specific capacity be realized in cathodes?

The existence of aluminum silicate inspires us the doping of Al³⁺ may be a correct choice. When part of [SiO₄]⁴⁻ has been replaced into [AlO₄]⁵⁻ in Li₂MnSiO₄, to compensate for the extra negative charge, corresponding lithium-ion is introduced and forms Li_{2+x}MnSi_{1-x}Al_xO₄, which leads a substantial increase of theoretical specific capacity ($\frac{(2+x)F}{3.6(161+6x)}$ mAh·g⁻¹, *F* is Faraday constant) in cathodes. The substitution

process can be described by the following defect equation:



Islam group once calculated the trivalent ion substitution on the Si site, and found the introducing additional lithium into Li₂MnSiO₄ was feasible¹⁷. Nevertheless, to our best knowledge, there have been few reports on the synthesis of Li_{2+x}MnSi_{1-x}Al_xO₄ cathodes⁸, probably since the substitution of [AlO₄]⁵⁻ tetrahedron instead of [SiO₄]⁴⁻ tetrahedron decreases the structure stability of Li_{2+x}MnSi_{1-x}Al_xO₄. Here we develop a supercritical mixed solvothermal approach to fabricate Li_{2+x}MnSi_{1-x}Al_xO₄/C (0 < x < 0.09) nanoparticles. In this approach, the carbon coating (arising from the carbonization of ethanol) plays a pivotal role. Li_{2+x}MnSi_{1-x}Al_xO₄ are covered by the carbon coating, which not only increases the products' structure stability, but also improves the products' electrochemical properties.

Experimental

Li_{2+x}MnSi_{1-x}Al_xO₄/C (x = 0, 0.05, 0.07, 0.09) nanoparticles were synthesized by mixed solvothermal process. LiOH·H₂O, MnCl₂·4H₂O, SiO₂ (Cabosil) and AlCl₃·6H₂O were dissolved in 10 ml mixed solution of ethanol (5 ml) and water (15 ml) in a molar ratio of (2+x):1:(1-x):x. After being stirred for few minutes, the mixture was transferred and sealed into a 40 ml stainless steel autoclave and kept at 550 °C for 3 h, and then being cooled to room temperature naturally. The product was

centrifuged and washed with distilled water and absolute ethanol several times, and finally dried in vacuum at 60 °C for 5 h.

The phase structure of samples was examined by Powder X-ray diffraction (XRD; Philips X'pert MPD with Cu K α radiation, $\lambda = 1.5418 \text{ \AA}$). The morphology and size of samples were analyzed by high-resolution transmission electron microscopy (HRTEM; JEOL-2011, using an accelerating voltage of 200 kV). The chemical compositions of samples were determined by energy dispersive X-ray spectroscopy (EDX), inductive coupled plasma emission spectroscopy (ICP-ES; Optima 7000DV) and atomic absorption spectroscopy (AAS; AAAnalyst 800). The carbon content of samples was evaluated from thermal gravimetric analysis (TGA; DT-50) data.

Electrochemical tests were conducted with coin cells (type 2016). The cathode was fabricated by pasting 80 wt% active material, 10 wt% acetylene black, and 10 wt% polyvinylidene fluoride (PVDF) dissolved in N-methylpyrrolidone (NMP) onto Al foil by doctor blade technique, and then the foil was dried under vacuum at 100 °C for 12 h. Metallic lithium was used as the anode. The electrolyte was 1 M LiPF₆ in a 1:1 mixture of ethylene carbonate (EC)/dimethyl carbonate (DMC); the separator was Celgard 2400. All the cells were assembled in a glove box filled with pure argon. The cells were cycled on an Arbin BT2043 battery test system between 1.5 and 4.5 V versus Li⁺/Li.

Results and discussion

The XRD patterns of the as-prepared samples (Li_{2+x}MnSi_{1-x}Al_xO₄/C) with different ratios of Al doping are shown in Fig. 1, and the calculated lattice parameters and cell volumes from the XRD patterns are listed in table 1. The diffraction peaks of the product obtained without Al doping ($x = 0$) are well assigned to the orthorhombic phase Li₂MnSiO₄ (space group *Pmn*2₁, fig. 1a). The calculated lattice parameters and cell volumes are in agreement with the previous reports.¹⁸ Fig. 1b and c show the XRD patterns of Li_{2.05}MnSi_{0.95}Al_{0.05}O₄ and Li_{2.07}MnSi_{0.93}Al_{0.07}O₄, respectively. In the two cases, the additional Li⁺ ions have been introduced into Li₂MnSiO₄ along with a small amount of Al³⁺ ions doping ($x \leq 0.07$). The two products both maintain the orthorhombic structures. The increase of cell volumes can be attributed to the Li⁺

interstitial compensation and the larger ionic radius of Al^{3+} (0.5 Å) than Si^{4+} (0.41 Å). At $x = 0.09$, the crystal structure of $\text{Li}_{2.09}\text{MnSi}_{0.91}\text{Al}_{0.09}\text{O}_4$ shifts to the monoclinic phase (fig. 1d),¹⁹ which indicates the higher doping concentration be able to change the crystal structure of $\text{Li}_{2+x}\text{MnSi}_{1-x}\text{Al}_x\text{O}_4$.

As listed in Table 2, the data derived from AAS, ICP-ES and EDX analysis confirm the chemical compositions of the $\text{Li}_{2+x}\text{MnSi}_{1-x}\text{Al}_x\text{O}_4$ samples. The results are close to the expected value.

Fig. 2a and b give the TEM images of $\text{Li}_{2.05}\text{MnSi}_{0.95}\text{Al}_{0.05}\text{O}_4/\text{C}$ and $\text{Li}_{2.09}\text{MnSi}_{0.91}\text{Al}_{0.09}/\text{C}$ nanoparticles, respectively. The two products both display irregular spherical polyhedron morphologies and relatively narrow size distributions. From Fig. 2c and d, one can see about 80% of the $\text{Li}_{2.05}\text{MnSi}_{0.95}\text{Al}_{0.05}\text{O}_4/\text{C}$ particles are in range of 7–12nm, with an average diameter of ca. 9 nm, and about 80% of the $\text{Li}_{2.09}\text{MnSi}_{0.91}\text{Al}_{0.09}/\text{C}$ particles are in range of 7–16nm, with an average diameter of ca. 11 nm.

The microstructures of $\text{Li}_{2.05}\text{MnSi}_{0.95}\text{Al}_{0.05}\text{O}_4/\text{C}$ composites were further investigated by HRTEM (Fig. 3a). By analyzing the image contrast, we deduced the dark core part is a $\text{Li}_{2.05}\text{MnSi}_{0.95}\text{Al}_{0.05}\text{O}_4$ nanoparticle, and the well-resolved lattice planes illustrate that the nanoparticles are single crystalline and structurally uniform. The measured interplanar spacing is ca. 0.42 nm, which corresponds to the separation of {110} planes of orthorhombic phase $\text{Li}_{2.05}\text{MnSi}_{0.95}\text{Al}_{0.05}\text{O}_4$. Outside of the core region, the light part is a layer of carbon coating with 1-2 nm thickness. The amounts of the carbon coating are measured by TGA in air atmosphere. As shown in Fig. 3b, 12.4% weight loss corresponds to the presence of carbon. The first weight loss below 120 °C is probably due to evaporation of absorbed water on the the surface of cathode materials.

In our reaction system to fabricate $\text{Li}_{2+x}\text{MnSi}_{1-x}\text{Al}_x\text{O}_4$ cathode materials, the carbon, which roots in the carbonization of ethanol under supercritical conditions: $\text{C}_2\text{H}_5\text{OH} \rightarrow 2\text{C} + \text{H}_2\text{O} + 2\text{H}_2$,²⁰ plays an important role at least in three: (1) improving the structural stability of $\text{Li}_{2+x}\text{MnSi}_{1-x}\text{Al}_x\text{O}_4$: the comparative experiments without ethanol showed that no $\text{Li}_{2+x}\text{MnSi}_{1-x}\text{Al}_x\text{O}_4$ were obtained; (2) controlling the size and

morphology of products: the neonatal $\text{Li}_{2+x}\text{MnSi}_{1-x}\text{Al}_x\text{O}_4$ seeds were covered by the carbon coating, which blocked the growth of these seeds and generated $\text{Li}_{2+x}\text{MnSi}_{1-x}\text{Al}_x\text{O}_4/\text{C}$ nanoparticles;²¹ (3) enhancing the Li-ion diffusion and electronic conductivity.¹⁰

Supercritical fluid, which exhibits both a density close to that of liquid and high diffusivity and low viscosity similar to that of gas, is helpful for the formation nanoparticles.⁶ In our sealed system, the supercritical state can be easily realized and provides a constant environment for the formation $\text{Li}_{2+x}\text{MnSi}_{1-x}\text{Al}_x\text{O}_4/\text{C}$ nanoparticles.

The first charge–discharge curves for the samples at 0.05 C between 1.5 and 4.5 V are shown in Fig. 4a-d. In the initial cycle, the $\text{Li}_{2+x}\text{MnSi}_{1-x}\text{Al}_x\text{O}_4/\text{C}$ nanoparticles deliver a discharge capacity of more than $170 \text{ mAh}\cdot\text{g}^{-1}$, which demonstrates there is beyond one Li^+ ion exchange in per formula unit (fig. 4e). Moreover, the three aluminum silicate samples exhibit higher discharge capacity than that of silicate sample, and the increase of Li^+ ions exchange exceeds the amount of additional lithium, which reveals the $\text{Li}_{2+x}\text{MnSi}_{1-x}\text{Al}_x\text{O}_4$ ($x \neq 0$) not only present more lithium but also are in favor of the intercalation and deintercalation of Li^+ ions. That may be caused by the enlarged $\text{Li}_{2+x}\text{MnSi}_{1-x}\text{Al}_x\text{O}_4$ ($x \neq 0$) cell volumes, which expand the transfer channels and contribute to the ion diffusion in the electrode reaction.²² Furthermore, all the samples have similar voltage profiles with the two discharge potential plateaus at around 2.8 V and 3.2 V, and two charge potential plateaus at around 3.25 V and 4.2 V, which correspond to the Li^+ ions intercalation and deintercalation process, respectively.^{6,11} The two discharge/charge potential plateaus suggest the existence of two stage Li^+ ions intercalation/deintercalation process, which respectively originate from the $\text{Mn}^{2+}/\text{Mn}^{3+}$ and $\text{Mn}^{3+}/\text{Mn}^{4+}$ redox reactions.⁶

Figure 5 represents the cycle performance of the samples at 0.05 C between 1.5 and 4.5 V. The discharge capacity dramatically decreases at the second cycle. This phenomenon mainly results from the decomposition of the electrolyte and subsequent formation of an organic layer deposited on the surface of particles that occur in the low-potential region for transition metal oxides. The capacity fading rate becomes slow during the subsequent cycles. That can be attributed to the existence of the

carbon coating, which prevents direct contact between the active cathode materials and the electrolyte,²¹ and thus slows down the erosion of $\text{Li}_{2+x}\text{MnSi}_{1-x}\text{Al}_x\text{O}_4$ upon cycling. Among these samples, $\text{Li}_{2.05}\text{MnSi}_{0.95}\text{Al}_{0.05}\text{O}_4/\text{C}$ appears higher capacity retention than the other samples and $204 \text{ mAh}\cdot\text{g}^{-1}$ capacity can be retained after 50 cycles (fig. 5b). In our opinion, the introduction of aluminum decreases the crystal field splitting energy and Jahn-Teller effect of $[\text{MnO}_4]$ tetrahedron, which preserves the crystal structure of cathode materials during cycling. However, the substitution of $[\text{AlO}_4]^{5-}$ in place of $[\text{SiO}_4]^{4-}$ decreases the structure stability of $\text{Li}_2\text{MnSiO}_4$, so the excess aluminum doping is not conducive to the improvement of the cycle performance (fig. 5c and d).

The rate performance of the samples has been shown in Fig. 6. It is obvious that the $\text{Li}_{2.05}\text{MnSi}_{0.95}\text{Al}_{0.05}\text{O}_4/\text{C}$ exhibits an excellent discharge capability in any measured rate. We think that the improvement of the rate performance should be put in relation to monodisperse nanoparticles, conductive carbon coating and slight Jahn-Teller effect.

Conclusions

In summary, $\text{Li}_{2+x}\text{MnSi}_{1-x}\text{Al}_x\text{O}_4/\text{C}$ nanoparticles have been synthesized under supercritical fluid conditions. Benefiting from the enlarged cell volumes and ion diffusion channels, $\text{Li}_{2+x}\text{MnSi}_{1-x}\text{Al}_x\text{O}_4$ cathodes have not only the increased theoretical specific capacity but also the improved electrochemical properties. At $x=0.09$, the obtained $\text{Li}_{2.09}\text{MnSi}_{0.91}\text{Al}_{0.09}\text{O}_4/\text{C}$ nanoparticles display higher discharge capacity; at $x=0.05$, the obtained $\text{Li}_{2.05}\text{MnSi}_{0.95}\text{Al}_{0.05}\text{O}_4/\text{C}$ nanoparticles display lower capacity fading and better rate performance. The carbon coating promotes the formation of $\text{Li}_{2+x}\text{MnSi}_{1-x}\text{Al}_x\text{O}_4$ nanoparticles and accelerates electron and ion transportation. To develop $\text{Li}_{2+x}\text{MnSi}_{1-x}\text{Al}_x\text{O}_4$ into one of the practical cathode materials with high specific capacity, the further studies are required to improve their stability, reversibility and conductivity.

Acknowledgements

This study was supported by Zhengzhou Key Laboratory for Clean Energy (111PYFZX151) and Science and Technology Key Project from Education

Department of Henan Province (13A150186).

References

- 1 T. M. Bandhauer, S. Garimella and T. F. Fuller, *J. Electrochem. Soc.*, 2011, **158**, R1.
- 2 B. Scrosati, J. Hassoun and Y. K. Sun, *Energy Environ. Sci.*, 2011, **4**, 3287.
- 3 L. Lu, X. Han, J. Li, J. Hua and M. Ouyang, *J. Power Sources*, 2013, **226**, 272.
- 4 M.E. Arroyo y de Dompablo, U. Amador, J.M. Gallardo-Amores, E. Morán, H. Ehrenberg, L. Dupont, R. Dominko, *J. Power Sources*, 2009, **189**, 638.
- 5 D. Rangappa, K. D. Murukanahally, T. Tomai, A. Unemoto and I. Honma, *Nano Lett.*, 2012, **12**, 1146.
- 6 D. M. Kempaiah, D. Rangappa and I. Honma, *Chem. Commun.*, 2012, **48**, 2698.
- 7 S. Choi, S. J. Kim, Y. J. Yun, S. S. Lee, S. Y. Choi, H. K. Jung, *Mater. Lett.*, 2013, **15**, 113.
- 8 H. Duncan, D. Aboud, C. Maiocco, Y. Abu-Lebdeh, I. J. Davidson, *The 15th International Meeting on Lithium Batteries*, The Electrochemical Society, May 2010.
- 9 H. Zhao, X. Wu, Y. Li, J. Shen, J. Xu, *J. Chin. Chem. Soc.*, 2011, **39**, 1084.
- 10 T. Muraliganth, K. R. Stroukoff and A. Manthiram, *Chem. Mater.*, 2010, **22**, 5754.
- 11 K. Takashi and Y. Hideaki, *J. Nanosci. Nanotechnol.*, 2013, **13**, 2689.
- 12 Z. Peng, H. Miao, H. Yin, C. Xu and W. G. Wang, *Int. J. Electrochem. Sci.*, 2013, **8**, 903.
- 13 Y. Zhao, C. Wu, J. Li and L. Guan, *J. Mater. Chem. A*, 2013, **1**, 3856.
- 14 S. Aono, T. Tsurudo, K. Urita and I. Moriguchi, *Chem. Commun.*, 2013, **49**, 2939.
- 15 X. Li, Y. Liu, Z. Xiao, W. Guo and R. Zhang, *Ceram. Int.*, 2014, **40**, 289.
- 16 M. K. Devaraju, T. Tomai, A. Unemoto, I. Honma, *RSC Adv.*, 2013, **3**, 608.
- 17 N. Kuganathan, M. S. Islam, *Chem. Mater.*, 2009, **21**, 5196.
- 18 R. Dominko, M. Bele, M. Gaberscek, A. Meden, M. Remskar and J. Jamnik, *Electrochem. Commun.*, 2006, **8**, 217.
- 19 V. V. Politaev, A. A. Petrenko, V. B. Nalbandyan, B. S. Medvedev and E. S. Shvetsova, *J. Solid State Chem.*, 2007, **180**, 1045.
- 20 C. Czosnek, M. Drygas and J. F. Janik, *Compos. Interfac.*, 2005, **12**, 459.
- 21 M. Zhang, Q. Chen, Z. Xi, Y. Hou and Q. Chen, *J. Mater. Sci.*, 2012, **47**, 2328.
- 22 S. Zhang, Z. Lin, L. Ji, Y. Li, G. Xu, L. Xue, S. Li, Y. Lu, O. Toprakci and X. Zhang, *J. Mater. Chem.*, 2012, **22**, 14661.

Table 1 Calculated lattice parameters (a , b , c and β), cell volumes (V) and structural units per cell (Z) for orthorhombic ($x = 0, 0.05, 0.07$) and monoclinic ($x = 0.09$) $\text{Li}_{2+x}\text{MnSi}_{1-x}\text{Al}_x\text{O}_4$

Samples	a (Å)	b (Å)	c (Å)	β (degree)	V (Å ³)	Z
$\text{Li}_2\text{MnSiO}_4$	6.311	5.380	4.970	90.00	168.747	2
$\text{Li}_{2.05}\text{MnSi}_{0.95}\text{Al}_{0.05}\text{O}_4$	6.334	5.358	5.100	90.00	173.082	2
$\text{Li}_{2.07}\text{MnSi}_{0.93}\text{Al}_{0.07}\text{O}_4$	6.350	5.401	5.102	90.00	174.980	2
$\text{Li}_{2.09}\text{MnSi}_{0.91}\text{Al}_{0.09}\text{O}_4$	6.382	10.966	5.547	91.06	388.140	4

Table 2 Chemical composition of the $\text{Li}_{2+x}\text{MnSi}_{1-x}\text{Al}_x\text{O}_4$ samples ($x = 0, 0.05, 0.07, 0.09$)

Samples	Li	Mn	Si	Al
$\text{Li}_2\text{MnSiO}_4$	1.995	0.999	1.000	0.000
$\text{Li}_{2.05}\text{MnSi}_{0.95}\text{Al}_{0.05}\text{O}_4$	2.046	0.994	0.955	0.047
$\text{Li}_{2.07}\text{MnSi}_{0.93}\text{Al}_{0.07}\text{O}_4$	2.066	0.992	0.941	0.068
$\text{Li}_{2.09}\text{MnSi}_{0.91}\text{Al}_{0.09}\text{O}_4$	2.085	0.987	0.922	0.089

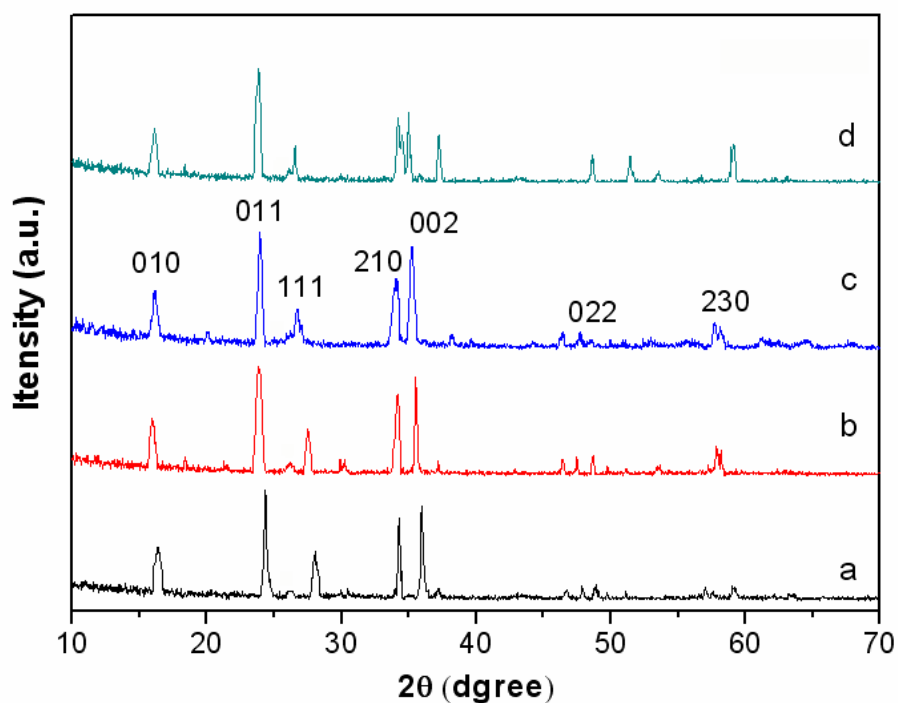


Fig. 1 XRD patterns of $\text{Li}_{2+x}\text{MnSi}_{1-x}\text{Al}_x\text{O}_4/\text{C}$ samples with (a) $x = 0$, (b) $x = 0.05$, (c) $x = 0.07$ and (d) $x = 0.09$

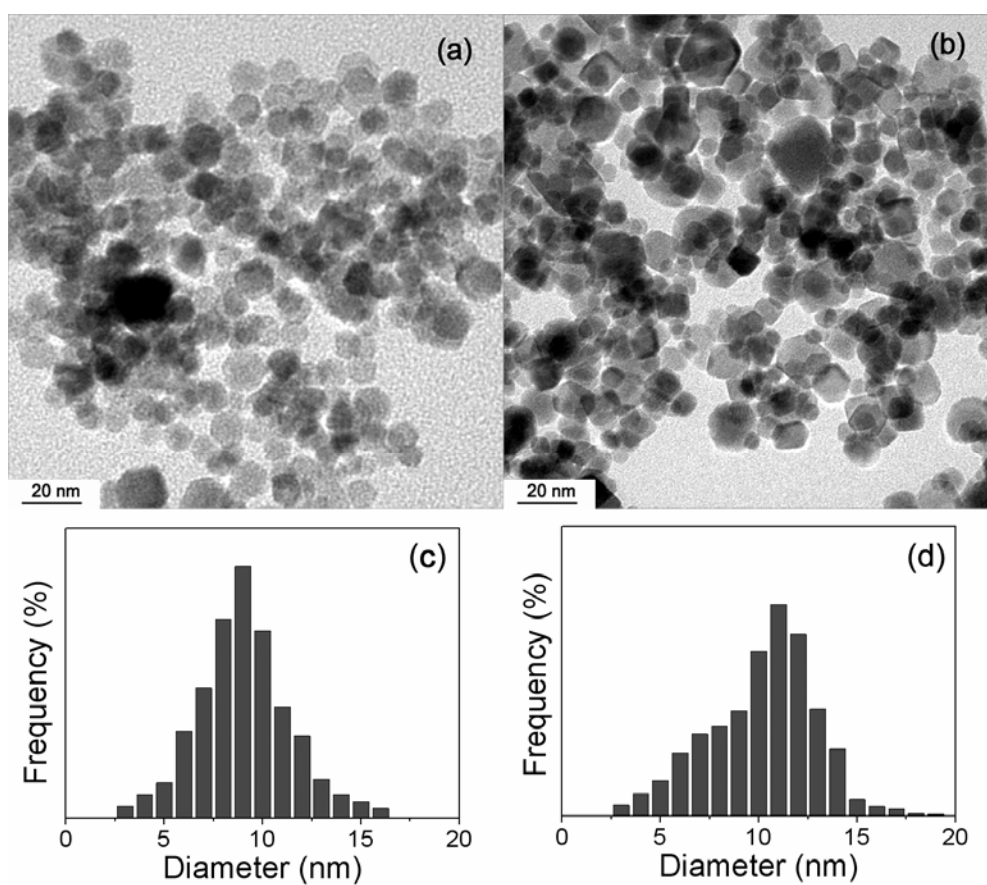


Fig. 2 TEM images of (a) $\text{Li}_{2.05}\text{MnSi}_{0.95}\text{Al}_{0.05}\text{O}_4/\text{C}$ and (b) $\text{Li}_{2.09}\text{MnSi}_{0.91}\text{Al}_{0.09}/\text{C}$; particle size distributions of (c) $\text{Li}_{2.05}\text{MnSi}_{0.95}\text{Al}_{0.05}\text{O}_4/\text{C}$ and (d) $\text{Li}_{2.09}\text{MnSi}_{0.91}\text{Al}_{0.09}/\text{C}$.

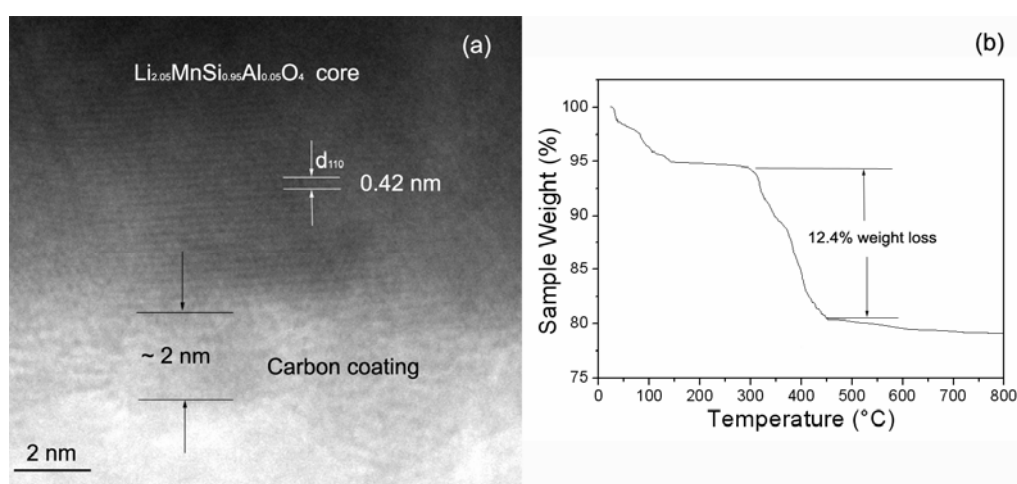


Fig.3 (a) HRTEM image of $\text{Li}_{2.05}\text{MnSi}_{0.95}\text{Al}_{0.05}\text{O}_4/\text{C}$; (b) TGA curve of $\text{Li}_{2.05}\text{MnSi}_{0.95}\text{Al}_{0.05}\text{O}_4/\text{C}$.

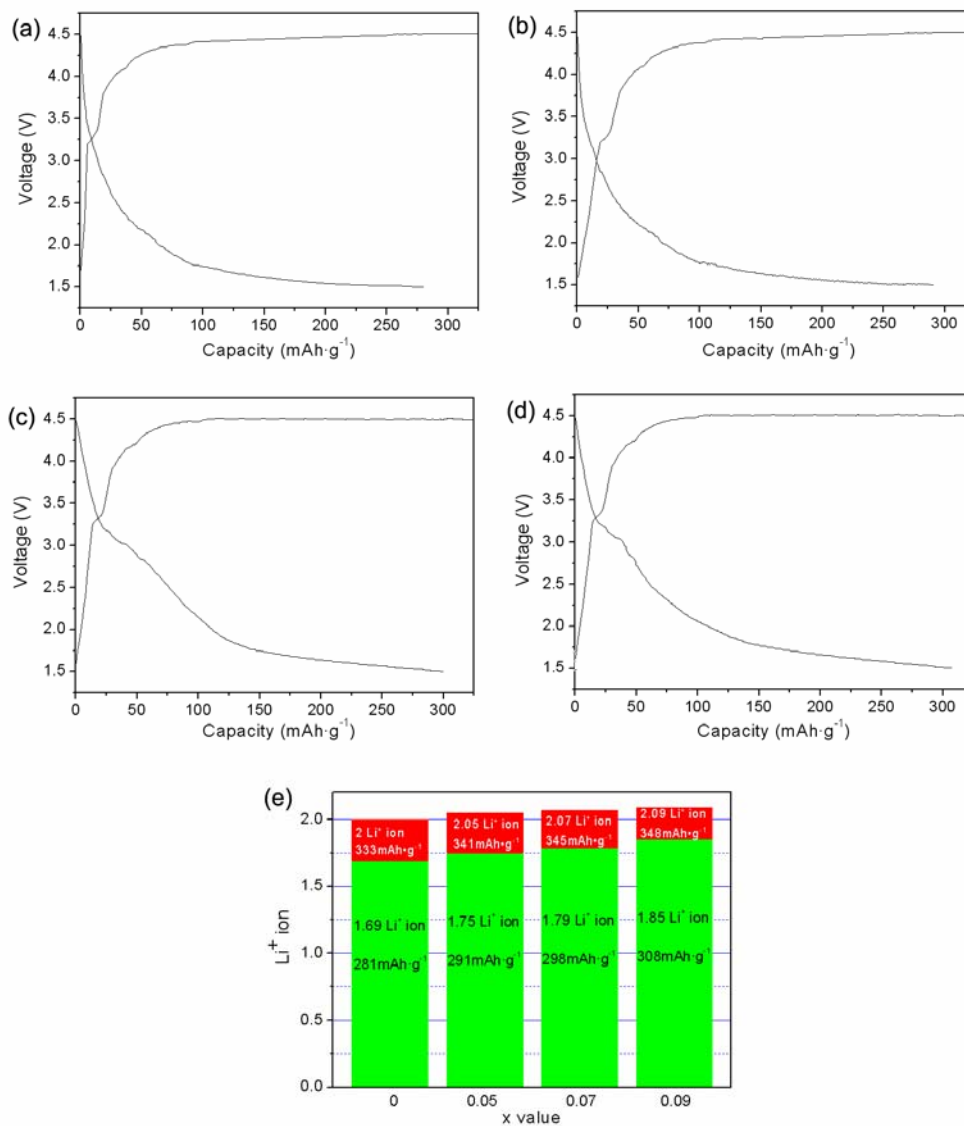


Fig. 4 The first charge–discharge curves of $\text{Li}_{2+x}\text{MnSi}_{1-x}\text{Al}_x\text{O}_4/\text{C}$ samples with (a) $x = 0$, (b) $x = 0.05$, (c) $x = 0.07$ and (d) $x = 0.09$ at 0.05 C ; (e) graphic illustration of the number of Li^+ ion exchange in per $\text{Li}_{2+x}\text{MnSi}_{1-x}\text{Al}_x\text{O}_4$ unit and corresponding discharge capacity while the first discharging (green column is the experimental value, and red column is the theoretical value.).

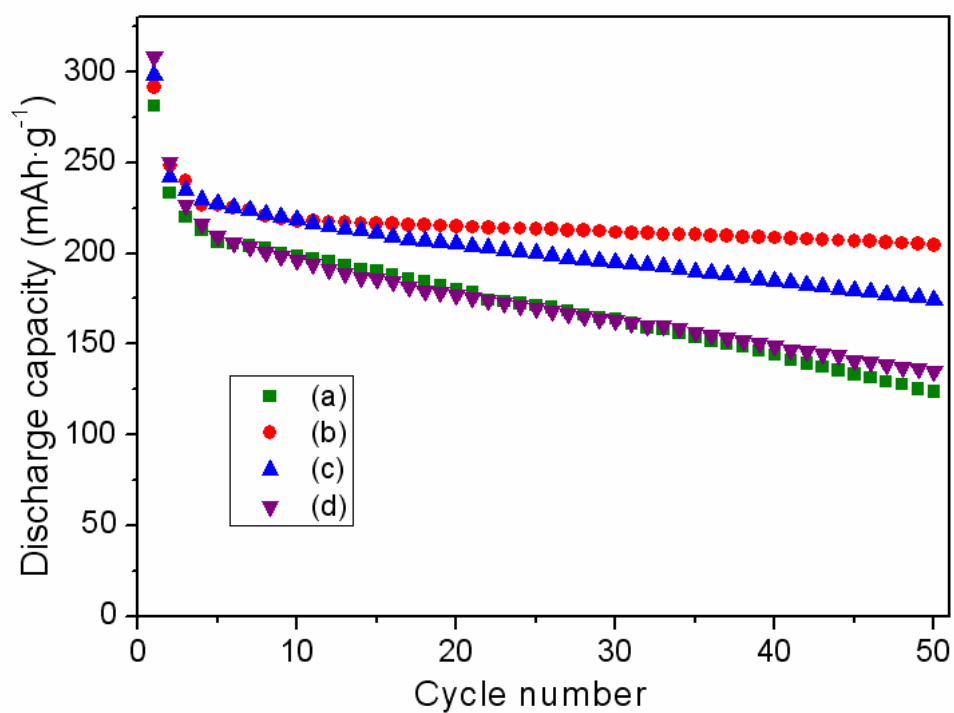


Fig. 5 Cyclic performance of $\text{Li}_{2+x}\text{MnSi}_{1-x}\text{Al}_x\text{O}_4/\text{C}$ samples with (a) $x = 0$, (b) $x = 0.05$, (c) $x = 0.07$ and (d) $x = 0.09$ at 0.05 C .

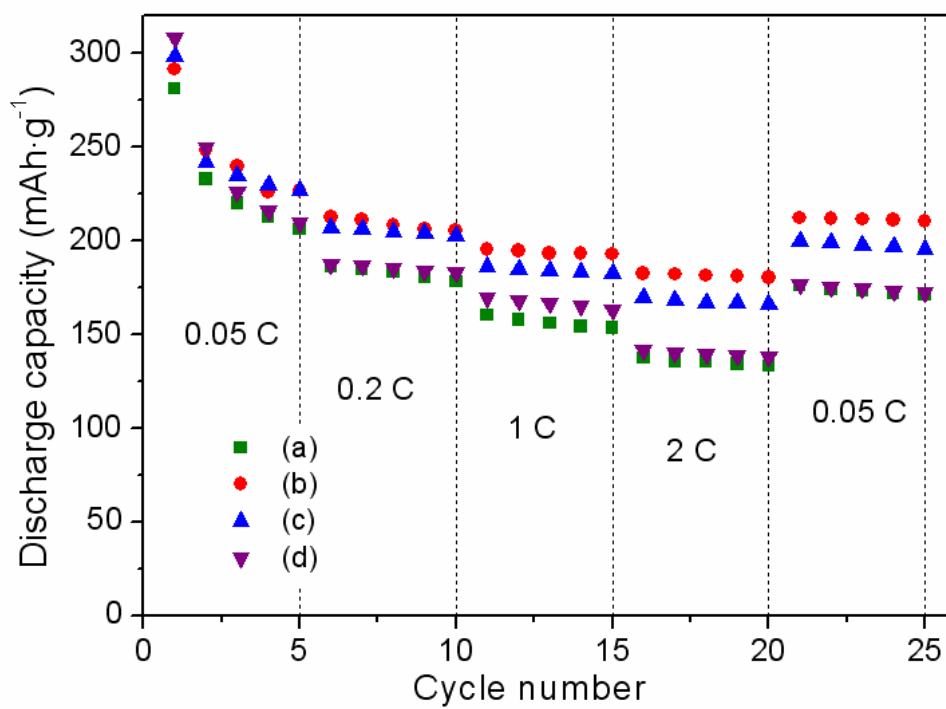


Fig. 6 Rate performance of $\text{Li}_{2+x}\text{MnSi}_{1-x}\text{Al}_x\text{O}_4/\text{C}$ samples with (a) $x = 0$, (b) $x = 0.05$, (c) $x = 0.07$ and (d) $x = 0.09$.